Soft Matter

PAPER

View Article Online
View Journal | View Issue

Cite this: *Soft Matter*, 2022, **18**, 322

Rigidity and fracture of biopolymer double networks†

Pancy Lwin,[d] Andrew Sindermann,[a] Leo Sutter,[a] Thomas Wyse Jackson,[b] Lawrence Bonassar,[c] Itai Cohen[b] and Moumita Das *[a]

Received 31st May 2021,
Accepted 24th November 2021

DOI: 10.1039/d1sm00802a

rsc.li/soft-matter-journal

Tunable mechanics and fracture resistance are hallmarks of biological tissues whose properties arise from extracellular matrices comprised of double networks. To elucidate the origin of these desired properties, we study the shear modulus and fracture properties of a rigidly percolating double network model comprised of a primary network of stiff fibers and a secondary network of flexible fibers. We find that when the primary network density is just above its rigidity percolation threshold, the secondary network density can be tuned to facilitate stress relaxation *via* non-affine deformations and provide mechanical reinforcement. In contrast, when the primary network is far above its rigidity threshold, the double network is always stiff and brittle. These results highlight an important mechanism behind the tunability and resilience of biopolymer double networks: the secondary network can dramatically alter mechanical properties from compliant and ductile to stiff and brittle only when the primary network is marginally rigid.

Introduction

Composite fiber networks are ubiquitous in biological systems and synthetic materials with tunable and robust mechanical properties. For example, the cytoskeleton, the scaffolding that gives eukaryotic cells mechanical integrity and shape, is a self-organized composite network of protein filaments, including actin and microtubules[1]. The distinct rigidity of actin and microtubules enables cells to exhibit complex stress responses and architectures essential for a wide range of functions.[2–5] As another example, the load-bearing capability of musculoskeletal tissues such as articular cartilage arises from a network-like extracellular matrix made of collagen fibers and proteoglycans.[6–9] Finally, several synthetic double network hydrogels have recently emerged as extraordinarily robust materials with considerable toughness and fracture resistance compared to conventional single network hydrogels. For instance, the PAMPS-PAAm double network hydrogel, which consists of interacting networks of poly(2-acrylamide-2-methylpropane sulfonic acid) and polyacrylamide, has a tearing energy $\sim$4400 J m^{-2}, which is several hundred to a thousand times that of single network PAAm and PAMPS hydrogels.[10,11] The exceptional mechanical response of these double network systems derives from the synergistic interplay between two networks with very different single-filament and collective properties.

The rigidity of stiff networks made of a single type of fiber or biopolymer, henceforth called single networks (SN), has been vigorously investigated in the past two decades, uncovering mechanical phase transitions, distinct mechanical regimes, and novel non-linear mechanical properties.[12–21] More recently, studies of the fracture mechanics of such networks have demonstrated that low network connectivity and system-wide distribution of damage can provide protective mechanisms against failure.[22,23] The mechanics and fracture of composite networks and materials, on the other hand, are only beginning to be explored theoretically, spanning systems such as composites materials made of rod-like inclusions in an SN,[24,25] composite networks,[26] and continuum models of double network hydrogels.[10] The mechanical structure-function properties of Double Networks (DNs)[27,28] are less well understood, and there remain many open questions as to the mechanisms by which DNs achieve such remarkable mechanical performance. In particular, it is unknown how much the second network can affect the rigidity percolation threshold for the combined DN system, an important parameter for setting the stiffness. Nor is it known to what degree the second network can tune the strain necessary for network failure (extensibility), the maximum stress reached (strength), and the energy density of mechanical deformation until failure (toughness) under extension, all of

[a] *School of Physics and Astronomy, Rochester Institute of Technology, Rochester, New York 14623, USA. E-mail: modsps@rit.edu*
[b] *Department of Physics, Cornell University, Ithaca, NY 14853, USA*
[c] *Meinig School of Biomedical Engineering and Sibley School of Mechanical and Aerospace Engineering, Cornell University, NY 14853, USA*
[d] *School of Mathematical Sciences, Rochester Institute of Technology, Rochester, NY 14623, USA*

† Electronic supplementary information (ESI) available. See DOI: 10.1039/d1sm00802a

which are important for determining the workable range of strains and stresses over which the system maintains its integrity. Addressing these questions will help guide the rational design of biomimetic soft materials with tunable mechanics and provide insights into the rigidity and fracture-resistance of load-bearing tissues such as cartilage.[29,30]

Here, we address these questions by combining two structure-function frameworks, (i) a DN made of two interacting disordered networks with very distinct fiber mechanics and (ii) rigidity percolation theory to construct a Rigidly Percolating Double Network model. Rigidity percolation theory models a biopolymer network as a disordered network of fibers consisting of flexible, sparsely connected regions and stiff, densely connected regions.[12,18,31–33] When the network consists primarily of sparsely connected regions, it does not offer any resistance to shear deformations and has zero shear modulus. In contrast, when densely connected regions span the network, the network has a finite shear modulus. The system undergoes a mechanical phase transition from non-rigid to rigid at a certain fiber density known as the rigidity percolation threshold.

The rigidly percolating double network model is made of a stiff primary network interacting with a flexible secondary network (Fig. 1(a)). In the stiff network, it costs energy to both stretch and bend fibers, while for the flexible network it only costs energy to stretch fibers. We study the shear response and crack propagation in this DN and show that the interplay of the mechanically distinct networks facilitates tunable mechanics and enhanced fracture resistance of the DN. Each of the two networks in the DN is modeled as a disordered kagome network and is constructed following the protocol described in Simulation Details. The bonds in the two networks are randomly removed according to two different probabilities, $1 - p_1$ for the stiff network, and $1 - p_2$ for the flexible network, where $0 < p_1, p_2 < 1$ are the bond occupation probabilities. A series of collinear bonds connected end to end constitute a fiber in each network. The stretching modulus of the fibers in the stiff and flexible networks are α_1 and α_2, respectively, where $\alpha_1 > \alpha_2$, and the bending modulus of the fibers in the stiff network is κ_1. The two networks interact with each other *via* Hookean springs with spring constant α_3 between the midpoints of the corresponding bonds in the networks; for this interaction to be non-zero the corresponding bonds must be present in both networks. See Fig. 1(b) for illustration of the properties of the bonds in the networks. Unless otherwise noted, we have used the following biologically relevant parameters in the results presented: $\alpha_2/\alpha_1 = 0.1$, $\kappa/\alpha_1 = 0.004$,[31] and $\alpha_3 = \alpha_1 + \alpha_2$ chosen to be the effective spring constant of two springs α_1 and α_2 in parallel. Simulations for smaller values of α_3 yielded qualitatively similar results and the percolation thresholds were unchanged. These results are discussed in the ESI.†

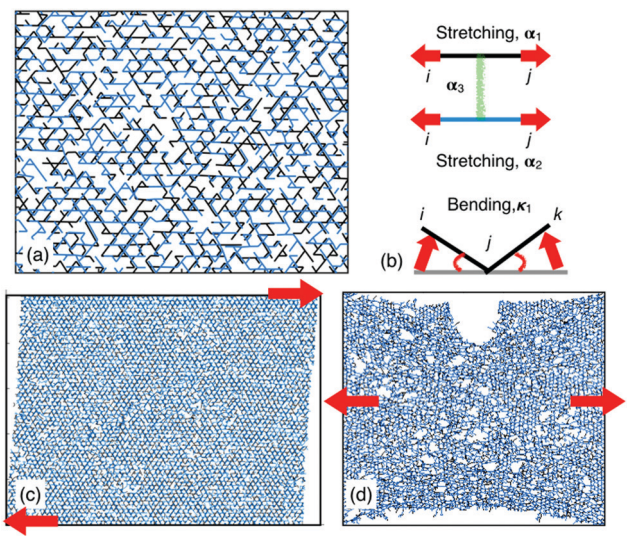

Fig. 1 Panel (a) represents a schematic of a zoomed-in portion of the DN, and (b) the different contributions to its deformation energy. The black and blue fibers belong to the the stiff and flexible networks respectively. Panels (c) and (d) show representative DNs (with $p_1 = 0.62$, $p_2 = 0.6$) for our studies of shear response and crack propagation respectively.

Model and method

Rigidly percolating double network model

The rigidly percolating double network model is made of two disordered networks, a stiff network and a flexible network, interacting with each other. Each network is constructed by following the protocol described in ref. 31 where we lay down infinitely long fibers in two dimensions in a Kagome lattice-based network, *i.e.* we start with a fully ordered lattice. To create a broad distribution of filament lengths, bonds are removed uniformly and in an uncorrelated manner from each network with a given probability: $0 < p_1 < 1$ for the stiff network and $0 < p_2 < 1$ for the flexible network. The bond occupation probabilities p_1 and p_2 can be tuned independently of each other. Within each network, when two fibers cross, we assume a crosslink such that the two crossing fibers can rotate freely but cannot slide relative to each other. Stretching energy of a network is calculated by computing the energy cost stretching or compression of individual bonds and then summing over all the bonds present in the network. Bending energy of a network is calculated by computing the energy of bending of pairs of bonds sharing a node which make a 180 degree angle in the initially undeformed network, and then summing over contributions from all such pairs of bonds present.

The total energy cost of deforming this double network is given by:

$$E_1 = \frac{\alpha_1}{2}\sum_{\langle ij\rangle} p_{1,ij}\left(\|r_{ij}\| - \|r_{ij0}\|\right)^2 + \frac{\kappa_1}{2}\sum_{\langle \widehat{ijk=\pi}\rangle} p_{1,ij}\, p_{1,jk}\, \Delta\theta_{ijk}^2 \quad (1)$$

$$E_2 = \frac{\alpha_2}{2}\sum_{\langle ij\rangle} p_{2,ij}\left(\|s_{ij}\| - \|s_{ij0}\|\right)^2$$

$$E_3 = \frac{\alpha_3}{2}\sum p_{1,ij}\, p_{2,ij}\left(\|x_1 - x_2\|\right)^2,$$

where E_1 is the deformation energy of the stiff network, E_2 is the deformation energy of the flexible network, and E_3 is the deformation energy of the bonds connecting the two networks which are modeled as Hookean springs as mentioned earlier. In E_1, the first term corresponds to the energy cost of fiber stretching, and the second term to fiber bending.[31] In E_2, we have a similar contribution for fiber stretching, but there is no energy cost of fiber bending. The indices i, j, k refer to sites (nodes) in each lattice based network, such that p_{ij} is 1 when a bond between those lattice sites is present, 0 if a bond is not present. The quantities $\mathbf{r}_{ij}$ and $\mathbf{s}_{ij}$ refer to the vector lengths between lattice sites i and j for the deformed stiff and flexible networks respectively, while $\mathbf{r}_{ij0}$ and $\mathbf{s}_{ij0}$ are the corresponding quantities for the initial undeformed networks. The angles $\Delta\theta_{ijk}$ correspond to the change in the angles between initially collinear bond pairs ij and jk for the deformed and undeformed network respectively.

Simulation details

Each network in our double network model consists of 10 619 nodes and 21 000 bonds when all bonds are present, not counting the connections between the two networks. The system size was chosen to be large enough so that the normalized shear modulus G/G_0 (where G_0 is the network shear modulus when the bond occupation probabilities are both 1) changed minimally with system size, but at the same time not so large that simulations become computationally prohibitive for very floppy networks. The rest length of bonds in each network is 1, *i.e.* this length scale is used to non-dimensionalize all lengths in the system. Similarly, all rigidities are expressed relative to the stretching modulus α_1. In our simulations, we assume a scaled bending to stretching elasticity ratio $\kappa/\alpha_1 = 0.004$ for the fibers in the stiff network.[31] We assume the ratio of the stretching elasticity of fibers in the flexible network to that of the stiff network to be $\alpha_2/\alpha_1 = 0.1$. The scaled interaction strength between the two networks α_3/α_1 is varied across the range $\sim$0.001–1, We used fixed boundaries at the top and bottom and apply deformations *via* these boundaries, and periodic boundaries on the sides. Upon application of the shear or extensional deformations, we obtain the equilibrium state of the deformed networks by minimizing the total deformation energy of the double network. The numerical method we used here is a multi-dimensional conjugate gradient (Polak–Ribiere) method.[34] Data are averaged over five simulations unless otherwise indicated.

Results

For the shear response studies (Fig. 1(c)), we adopt a protocol where external deformations are applied along the top and bottom boundaries and periodic boundary conditions are used for the left and right sides of the network. Our simulations of the single network follow the same process, except the deformation energy consists only of contribution from the stiff primary network, since $p_2 = 0$. To obtain the linear mechanical response, we apply a shear strain of 5% at the boundaries, minimize the deformation energy using a multi-dimensional conjugate gradient minimization (Polak–Ribiere) method[34] and calculate the shear modulus.[31]

We show the variation of the rigidity percolation threshold of a single network (SN) and four DNs by plotting the shear modulus *versus* bond occupation probability of the stiff network p_1 (Fig. 2). The shear moduli G are normalized by their respective values G_0 for fully occupied networks. The four DNs correspond to the four different values of the bond occupation probability $p_2 = 0.2, 0.4, 0.6, 0.8$ of the flexible network. We find that the SN has a percolation threshold $p_{1,c} \sim 0.6$ in agreement with previous results,[35] while the DNs have a lower $p_{1,c}$, which decreases with increasing p_2, reaching $p_{1,c} \sim 0.35$ at $p_2 = 0.8$. This is a noteworthy result. On its own, a single stiff Kagome-lattice based fiber network, whose deformation energy consists of stretching and bending energies, has a percolation threshold $\sim$0.6,[35] and a single flexible network with only stretching deformation energy and based on such a lattice has a percolation threshold $\sim$1. However, when they form a double network, the resulting additional constraints due to their interaction lead to a lower, tunable percolation threshold. These constraints also allow the normalized shear rigidity of the DNs to be larger than that of the SN at the same value of p_1, and this rigidity can be tuned by varying p_2. This result illustrates a mechanism for how the onset of rigidity for biological and synthetic double networks can be drastically modulated through very small changes in filament concentration in the secondary network.

For the crack propagation studies (Fig. 1(d)), we create a notch 20 times the bond rest length ($\sim$1/5 times the system length) at the center of the top boundary following the protocol in ref. 36, and study how the size of the notch increases as we

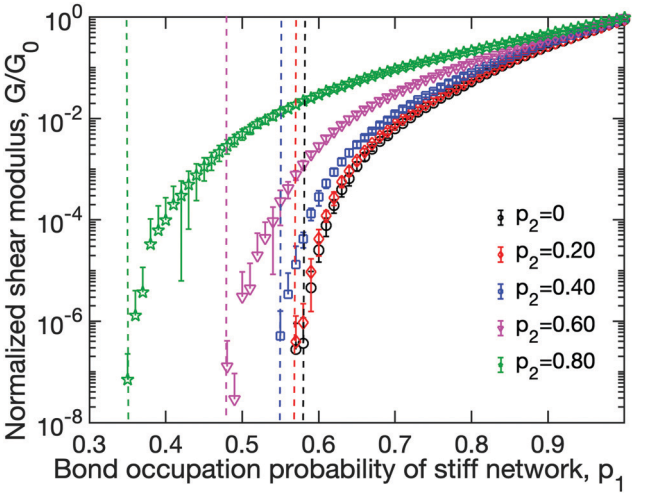

Fig. 2 The normalized shear modulus (G/G_0) shown as a function of p_1 for an SN (black circles) and four DNs (remaining data). The values of p_2 are shown in the legend. The dashed lines provide guide to the eye for the rigidity percolation transitions. The data is averaged over five runs and the standard deviations are indicated by errorbars.

apply larger and larger tensile strains along the left and right boundaries of the network.

The strains are applied quasi-statically in small increments of 1% up to 70%, and after each application, the total energy is minimized to generate the new equilibrium configuration of the deformed DN. We have made the following assumptions regarding breaking and elastic buckling of fibers: when a bond is stretched above a certain threshold, it will break, and when it is compressed above a certain threshold, it will buckle. Bonds in the stiff network break at 120% of their rest length and buckle at 95% of their rest length. Bonds in the flexible network break at 200% of their rest length, but do not buckle. Broken or buckled bonds will no longer contribute to the deformation energy or rigidity of the network. Fiber breaking is an irreversible process, but buckled fibers in our model can "unbuckle" when the extra compression is removed.

To demonstrate how the fracture mechanics changes with the stiff network's proximity to its rigidity percolation threshold, we present results for simulations of the DN close to (p_1 = 0.62) and away from (p_1 = 0.80) the rigidity threshold (Fig. 3). The values of p_1 were chosen, so that the DN has a finite rigidity, irrespective of p_2.‡ We find that both the Young's modulus (Fig. 3(a) and (b)) as well as the stress (Fig. 3(c) and (d)) developed in the network initially increase with strain and reach a maximum as previously floppy regions become stretched and align to resist deformation. Once the fibers in the network start to experience strains larger than their stretching (or elastic buckling) thresholds, however, they break (or buckle), causing the network to soften. Remarkably, we find that when the stiff network is close to its rigidity threshold, the normalized Young's modulus, the maximum or peak stress, and the strain at maximum stress (onset of failure), can be shifted dramatically by the flexible network. This tunability arises because the sparsely populated stiff network allows the DN to undergo non-affine rearrangements,[13,17,18] leading to large variations in rigidity. The mechanics can be further varied using the coupling between the two networks in the DN (see ESI†).

We quantify these trends by comparing the peak stress σ_p, strain at maximum stress $\gamma(\sigma = \sigma_p)$, and the fracture toughness τ *versus* p_2 for both DNs in Fig. 3. Here we have used the total area under the stress–strain curve as a measure of the network's fracture toughness. We find that the peak stress increases with p_2 for both DNs due to the additional constraints introduced by the secondary, flexible network. The strain at maximum stress decreases with p_2 when the stiff network is close to the percolation threshold and remains nearly constant when the stiff network is far from the percolation threshold. Thus, the additional constraints introduced by the secondary network play a much greater role in restricting deformation when the stiff network is near the rigidity percolation threshold. Finally, we find that while the network toughness increases for both cases, the increase is greater for the network near the rigidity percolation threshold. This result is somewhat surprising. The measure of toughness used here is typically proportional to the product of the peak stress and strain at the onset of failure where the material fails abruptly. Here, while this product remains nearly constant for the p_1 = 0.62 data as p_2 in varied, the measured area under the stress–strain curve increases with p_2. This is because as the network fails gradually, the decrease in stress is far less abrupt than in typical materials, and the network toughness is substantially increased.

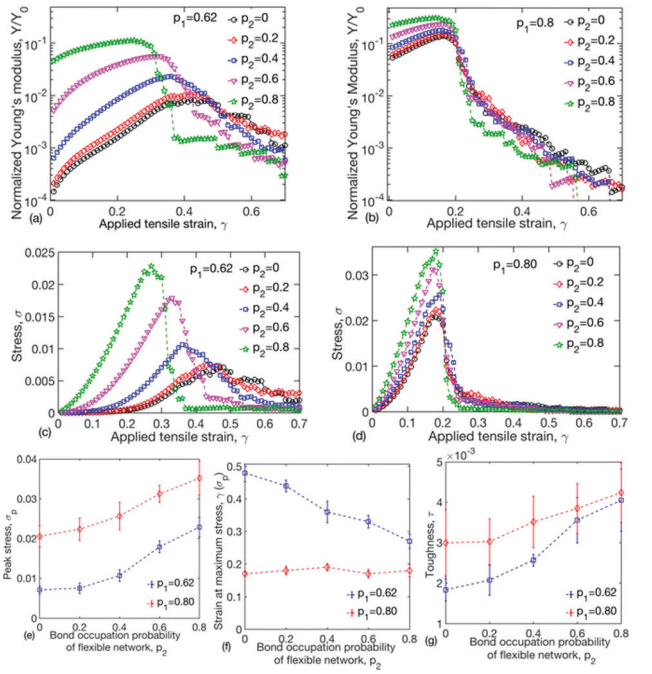

Fig. 3 (a and b) Show the normalized Young's modulus Y/Y_0 and (c and d) show the stresses σ developed in the SN (black circles) and DN (remaining data) as a function of the uniaxial tensile strain γ applied at the boundaries. (a) and (c) Corresponds to p_1 = 0.62, and (b) and (d) to p_1 = 0.80; p_2 is as shown in the legend in these figures. (e)–(g) show the peak stress (σ_p), and the strain at peak stress ($\gamma(\sigma_p)$), and the toughness (τ) as a function for p_2 for the data shown in (c) and (d). The stress is expressed in units of $\alpha_1 \times \rho$, where ρ is network concentration in total fiber length per volume for the stiff network, and the toughness, which is the total area under the stress–strain curves shown in (c) and (d), has the same unit. The data is averaged over five runs and the standard deviations are indicated by errorbars.

Conclusion

These results highlight an important and novel mechanism in shear and fracture mechanics of DN polymer systems: a secondary flexible network can be used to dramatically tune the mechanics of a composite DN when the primary stiff network is just above the rigidity percolation threshold. In this regime, decreasing p_2 allows internal stresses to relax through non-affine deformations and enables the DN to remain intact until larger strains, while increasing p_2 leads to larger mechanical reinforcement from the secondary network. The results show how the DN can be modulated to either be extensible, breaking gradually, as is the case for low p_2 or be stronger, breaking in a

‡ We found, for example, that when p_1 was set to 0.55, the DN had zero shear rigidity and exhibited no stresses when p_2 was 0, 0.2, or 0.4

more brittle fashion, as is the case for high p_2. In contrast, far above the rigidity threshold, the primary stiff network is far too dense and rigid to allow any non-affine network restructuring or rearrangement of the DN by varying the density of the secondary flexible network; the DN is brittle, and breaks before stresses can be dissipated. The low p_2 limit is particularly important in biological tissues such as articular cartilage when it is undergoing osteoarthritis, where the proximity of the stiff (collagen) network to the rigidity percolation threshold varies as a function of tissue depth and the reinforcing flexible network is increasingly removed as the disease progresses.[31,37,38]

To illustrate the above-mentioned mechanism visually, we present stills from simulations of crack propagation in DNs with p_1 = 0.62 and 0.80 as a function of the applied tensile strain γ and p_2 (Fig. 4). We find that when the stiff network is far above the rigidity threshold (p_1 = 0.80, Fig. 4(a)), the DN ruptures abruptly at $\gamma \sim 0.2$ for all p_2 values, though the crack morphology is more uniform at higher p_2. In contrast, when the stiff network is close to the rigidity threshold (p_1 = 0.62, Fig. 4(b)), we observed a wider range of responses. For p_2 = 0, 0.2, and 0.4 the networks are extensible, initially developing microcracks that are distributed throughout. With increasing strain, these microcracks grow and the network decreases its rigidity while maintaining a percolated structure. For p_2 = 0.6 and 0.8 the networks are more brittle, rupturing less homogeneously and maintaining their rigidity up until the point of failure.

Importantly, this ability to tune the failure characteristics could have numerous important applications. For example, our simulations suggest that it may be possible to construct DNs with varying compositions to guide the trajectory or even stall cracks propagating through the material. We speculate, given the similarity of some of the crack morphologies in our simulations (*e.g.*, p_2 = 0.6, γ = 0.35 in Fig. 4b) to the experimentally observed fracture of articular cartilage tissue (see for example Fig. 4 in ref. 36) it is possible that cartilaginous tissues may already be employing such mechanisms.

Over the last decade, double network systems have become technologically important because they have enhanced toughness, delayed gel fracture, and controllable peeling behaviors. Our results illustrate a mechanism that allows for controlling how much the secondary network can do to attenuate or relax stresses in the primary network, and can inform the choice of materials and microstructural parameters for the rational design of biomimetic soft composite materials with desired properties.

Finally, we note that the observed richness of behaviors presented here could be further enhanced by including additional tuning parameters such as non-linear elasticity, viscous dissipation, structural correlations, network hierarchy, network polarization or bond polydispersity in one or both of the networks of the double network. This flexibility in resulting material properties and ease of implementation make double networks a very attractive platform for the fabrication of mechanically tunable artificial tissue constructs. The results presented here are an important step towards achieving this future.

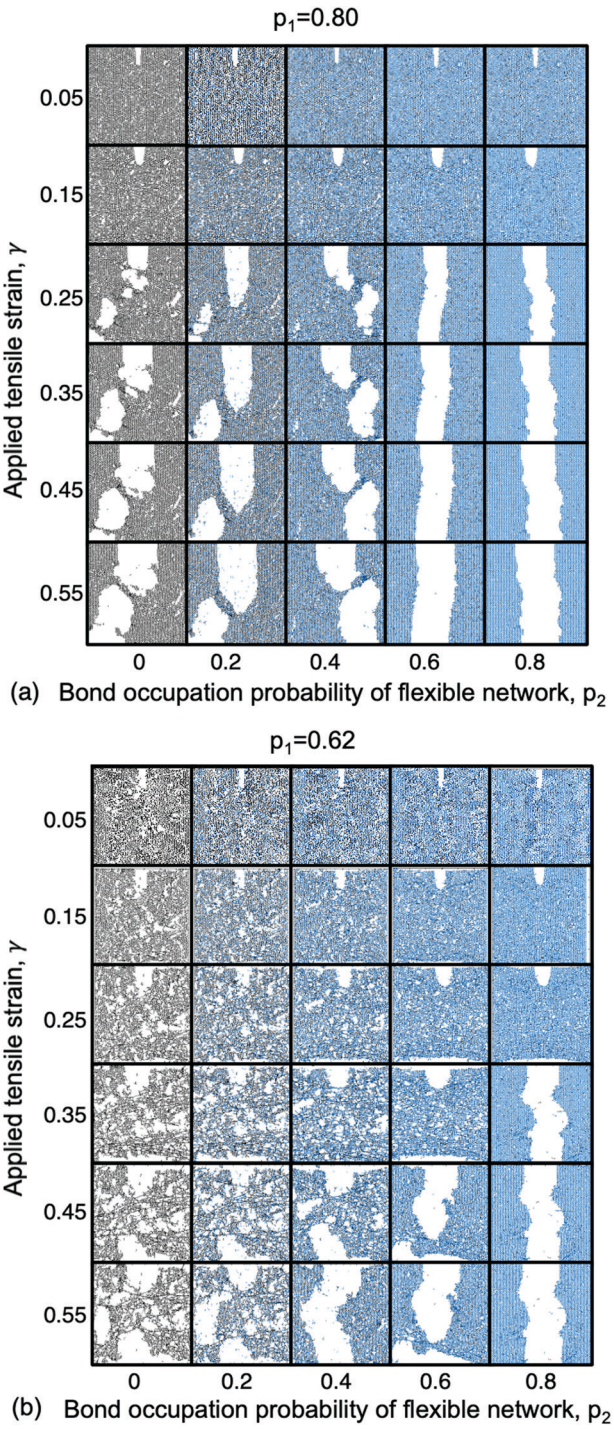

Fig. 4 Deformation and fracture of the SN (p_2 = 0) and the DN ($p_2 \neq 0$) as a function of increasing p_2 (x-axis) and applied strain (y-axis). The value of p_1 is set to 0.80 in (a) and to 0.62 in (b), *i.e.* the stiff network is just above the rigidity percolation threshold in (a) and far above this threshold in (b). Both the SN and DN were subjected to uniaxial strains applied at the boundary and the strain was increased in steps of 1%.

Conflicts of interest

The authors declare no competing interests.

Acknowledgements

The authors thank Jonathan Michel, Lisa Fortier, Guy Genin, Markus Linder, and Andrej Košmrlj for useful discussions. This research was supported in part by NSF grants DMR-1808026, CBET-1604712, DMR-1807602, and CMMI-1536463.

Notes and references

1 *The Cytoskeleton*, ed. T. D. Pollard and R. D. Goldman, Cold Spring Harbor Laboratory Press, 2017.
2 V. Pelletier, N. Gal, P. Fournier and M. L. Kilfoil, *Phys. Rev. Lett.*, 2009, **102**, 188303.
3 J. L. R. Shea, N. Ricketts and R. M. Robertson-Anderson, *Biophys. J.*, 2018, **115**, 1055–1067.
4 S. N. Ricketts, M. L. Francis, L. Farhadi, M. J. Rust, M. Das, J. L. Ross and R. M. Robertson-Anderson, *Sci. Rep.*, 2019, **9**, 12831.
5 G. Lee, G. Leech, P. Lwin, J. Michel, C. Currie, M. Rust, J. L. Ross, R. J. McGorty, M. Das and R. M. Roberston-Anderson, *Soft Matter*, 2021, DOI: 10.1039/D1SM01083B.
6 V. C. Mow, A. Ratcliffe and A. R. Poole, *Biomaterials*, 1992, **13**, 67–97.
7 Y. Fung, *Biomechanics: Mechanical Properties of Living Tissues*, Springer-Verlag, New York, 2nd edn, 1993.
8 S. W. O'Driscoll, *J. Bone Joint Surg. Am.*, 1998, **80**, 1795–1812.
9 J. H. Lai and M. E. Levenston, *Osteoarthritis Cartilage*, 2010, **18**, 1291–1299.
10 M. A. Haque, T. Kurokawa and J. P. Gong, *Polymer*, 2012, **53**, 1805–1822.
11 T. Nonoyama and J. P. Gong, *Polymer*, 2015, **229**, 853–863.
12 C. Broedersz, X. Mao, T. Lubensky and F. C. MacKintosh, *Nat. Phys.*, 2011, **7**, 983–988.
13 D. A. Head, A. J. Levine and F. C. MacKintosh, *Phys. Rev. E: Stat., Nonlinear, Soft Matter Phys.*, 2003, **68**, 061907-1-14.
14 J. Wilhelm and E. Frey, *Phys. Rev. Lett.*, 2003, **68**, 108103-1.
15 M. Gardel, J. Shin, F. MacKintosh, L. Mahadevan, P. Matsudaira and D. Weitz, *Phys. Rev. Lett.*, 2004, **93**, 188102.
16 A. R. Missel, M. Bai, W. S. Klug and A. J. Levine, *Phys. Rev. E: Stat., Nonlinear, Soft Matter Phys.*, 2010, **82**, 041907-1.
17 C. Heussinger and E. Frey, *Phys. Rev. Lett.*, 2006, **97**, 105501-1.
18 M. Das, F. C. Mackintosh and A. J. Levine, *Phys. Rev. Lett.*, 2007, **99**, 038101-1.
19 H. Kang, Q. Wen, P. A. Janmey, J. X. Tang, E. Conti and F. C. MacKintosh, *J. Phys. Chem. B*, 2009, **113**, 3799–3805.
20 M. Sheinman, C. P. Broedersz and F. C. MacKintosh, *Phys. Rev. E: Stat., Nonlinear, Soft Matter Phys.*, 2012, **85**, 021801-1.
21 R. C. Picu, *Soft Matter*, 2011, **7**, 6768–6785.
22 L. Zhang, D. Z. Rocklin, L. M. Sander and X. Mao, *Phys. Rev. Mater.*, 2017, **1**, 052602.
23 F. Burla, S. Dussi, C. Martinez-Torres, J. Tauber, J. van der Gucht and G. H. Koenderink, *Proc. Natl. Acad. Sci. U. S. A.*, 2020, **117**, 8326–8334.
24 M. Das, A. J. Levine and F. C. Mackintosh, *Europhys. Lett.*, 2008, **84**, 18003-1.
25 M. Das and F. C. MacKintosh, *Phys. Rev. Lett.*, 2010, **105**, 138102.
26 F. Burla, J. Tauber, S. Dussi, J. van der Gucht and G. H. Koenderink, *Nat. Phys.*, 2019, **15**, 549–553.
27 J. Tauber, S. Dussi and J. Van Der Gucht, *Phys. Rev. Mater.*, 2020, **4**, 063603.
28 D. S. Nedrelow, D. Bankwala, J. D. Hyypio, V. K. Lai and V. H. Barocas, *Acta Biomater.*, 2018, **72**, 306–315.
29 D. Trivedi, C. D. Rahn, W. M. Kier and I. D. Walker, *Appl. Bion. Biomech.*, 2008, **5**, 99–117.
30 D. Taylor, N. O'Mara, E. Ryan, M. Takaza and C. Simms, *J. Mech. Behav. Biomed. Mater.*, 2012, **6**, 139–147.
31 J. L. Silverberg, A. R. Barrett, M. Das, P. B. Petersen, L. J. Bonassar and I. Cohen, *Biophys. J.*, 2014, **107**, 1721–1730.
32 S. Feng, M. F. Thorpe and E. Garboczi, *Phys. Rev. B: Condens. Matter Mater. Phys.*, 1985, **31**, 276–280.
33 M. Das, D. A. Quint and J. M. Schwarz, *PLoS One*, 2012, **7**, e35939-1-11.
34 W. H. Press, S. A. Teukolsky, W. T. Vetterling and B. P. Flannery, *Numerical Recipes in Fortran 90: The Art of Scientific Computing*, Second Edition, Cambridge University Press, 1996.
35 X. Mao, O. Stenull and T. C. Lubensky, *Phys. Rev. E: Stat., Nonlinear, Soft Matter Phys.*, 2013, **87**, 042602.
36 K. Stok and A. Oloyede, *Connect. Tissue Res.*, 2003, **44**, 109–120.
37 D. J. Griffin, J. Vicari, M. R. Buckley, J. L. Silverberg, I. Cohen and L. J. Bonassar, *J. Orthop. Res.*, 2014, **32**, 1652–1657.
38 T. W. Jackson, J. Michel, P. Lwin, L. Fourtier, M. Das, L. J. Bonassar and I. Cohen, preprint, arXiv:2105.14018.